

# Electron-phonon interaction and charge carrier mass enhancement in SrTiO<sub>3</sub>

J.L.M. van Mechelen,<sup>1</sup> D. van der Marel,<sup>1</sup> C. Grimaldi,<sup>1,2</sup> A.B. Kuzmenko,<sup>1</sup>  
N.P. Armitage,<sup>1,3</sup> N. Reyren,<sup>1</sup> H. Hagemann,<sup>4</sup> and I.I. Mazin<sup>5</sup>

<sup>1</sup> *Département de Physique de la Matière Condensée, Université de Genève, Genève, Switzerland.*

<sup>2</sup> *LPM, Ecole Polytechnique Fédérale de Lausanne, Lausanne, Switzerland.*

<sup>3</sup> *Department of Physics and Astronomy, The Johns Hopkins University, Baltimore, USA.*

<sup>4</sup> *Département de Chimie Physique, Université de Genève, Genève, Switzerland.*

<sup>5</sup> *Center for Computational Materials Science, Naval Research Laboratory, Washington D.C., USA.*

We report a comprehensive THz, infrared and optical study of Nb doped SrTiO<sub>3</sub> as well as DC conductivity and Hall effect measurements. Our THz spectra at 7 K show the presence of a very narrow ( $< 2$  meV) Drude peak, the spectral weight of which shows approximately a factor of three enhancement of the band mass for all carrier concentrations. The missing spectral weight is regained in a broad ‘mid-infrared’ band which originates from electron-phonon coupling. We find no evidence of a particularly large electron-phonon coupling that would result in small polaron formation. Analysis of the results yields an electron-phonon coupling parameter of an intermediate strength,  $\alpha \approx 4$ .

PACS numbers: 71.38.-k, 72.20.-i, 78.20.-e

Electron-phonon coupling in the perovskites is a subject of much recent interest due to the controversy over its relevance in the phenomena of multiferroicity, ferroelectricity, superconductivity and colossal magnetoresistance [1, 2, 3, 4, 5]. Despite much progress, full understanding of the physics of electron-phonon coupling in perovskites is still lacking because of additional crystallographic complexities of many materials involved (breathing, tilting and rotational distortions, ferroelectric symmetry breaking), magnetism, complex electronic effects (strong correlations), and also because of the lack of high-accuracy spectroscopic measurements specifically designed to probe electron-phonon coupling.

With this in mind, we have studied a prototypical perovskite oxide, SrTi<sub>1-x</sub>Nb<sub>x</sub>O<sub>3</sub> with  $0 \leq x \leq 0.02$ . SrTiO<sub>3</sub> is an insulator ( $\Delta = 3.25$  eV) with the conduction band formed by the Ti 3d states. These are split by the crystal field so that the three  $t_{2g}$  states become occupied when the material is electron-doped by substituting pentavalent Nb for tetravalent Ti. For  $0.0005 \leq x \leq 0.02$  SrTi<sub>1-x</sub>Nb<sub>x</sub>O<sub>3</sub> becomes superconducting at a  $T_c$  of typically  $\sim 0.3$  K [6, 7], and at most 1.2 K [5]. Characterized by the threefold degeneracy of the conduction bands and the high lattice polarizability, electron doped SrTiO<sub>3</sub> provides a perfect opportunity for the study of electron-phonon coupling and polaron formation in an archetypal perovskite [8, 9].

One of the fingerprints of an ultrastrong electron-phonon coupling is the formation of small polarons that are observable in the form of a gigantic electron mass renormalization. The renormalized mass can be obtained by measuring the optical spectral weight of the Drude peak, which in proper units is equal to  $n/m^*$ . Besides renormalizing the ‘coherent’ (Drude) part of the spectrum, the electron-phonon coupling is responsible for the ‘incoherent’ contributions at higher energies, resulting in

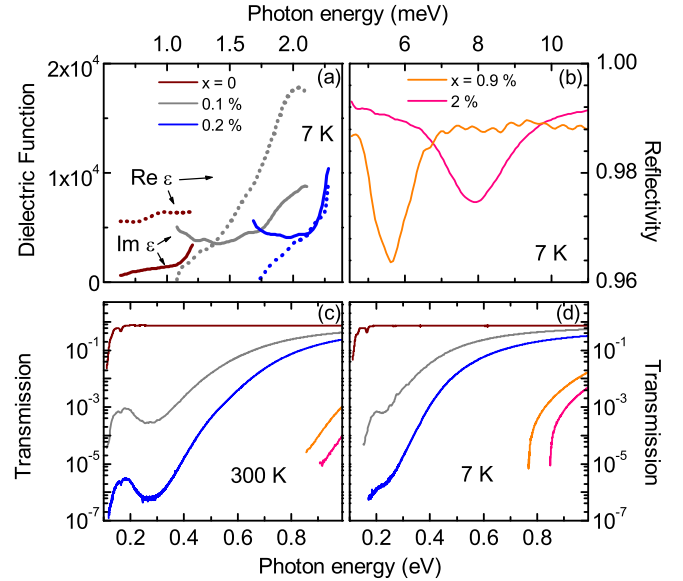


FIG. 1: Selected the experimental data. A very narrow Drude peak at 7K can be seen in both (a),  $\epsilon_1(\omega)$  (dotted curves) and  $\epsilon_2(\omega)$  (solid curves) in the THz range for  $x = 0.1\%$  and  $0.2\%$ , and (b), the upturn in the reflectivity at low energies for  $x = 0.9\%$  and  $2.0\%$ . (c-d), Transmission coefficient at (c), 300 K and (d), 7 K showing the absorption in the mid-infrared.

a multiphonon absorption band in the mid-infrared.

To address these issues, we have measured the optical reflectivity and transmission (Fig. 1) of double side polished,  $5 \times 5$  mm<sup>2</sup> ((100) face) single crystals of Sr<sub>1-x</sub>Nb<sub>x</sub>TiO<sub>3</sub> between 300 K and 7 K by time-domain THz spectroscopy (TPI spectra 1000, TeraView Ltd.), Fourier transform infrared spectroscopy and photometric IR-UV spectroscopy, between 0.3 meV and 7 eV. To obtain a detectable transmission we have used for each composition several samples of different thickness

(8 – 60  $\mu\text{m}$ ), adopted to the spectral range and value of the optical transmission. The Hall carrier concentrations were 0.105%, 0.196%, 0.875% and 2.00% at 7 K, which were within 5 % of those measured by the wavelength-dispersive X-ray spectroscopy, and within 12 % of the Nb concentration specified by the supplier (0.1%, 0.2%, 1.0% and 2.0%, respectively, Crystec, Berlin). Compared to earlier measurements [10, 11, 12, 13, 14], we expand the spectral range further into the far-infrared and THz band. Fig. 1a shows both components of the dielectric function,  $\epsilon_1(\omega)$  and  $\epsilon_2(\omega)$ , in the THz range at 7 K, as obtained by a direct inversion of the measured transmission amplitude and phase. From the DC resistivity, the reflectivity and the transmission data we calculated the real and imaginary part of the optical conductivity using a generalized Kramers-Kronig routine [15].

The only subgap contributions to the optical conductivity of undoped  $\text{SrTiO}_3$  (Fig. 2) are the three infrared active phonons at 11.0, 21.8 and 67.6 meV (at room temperature). The lowest one exhibits a strong red shift upon cooling, and saturates at about 2.3 meV at 7 K. Upon doping this mode hardens for all temperatures, reaching 8.5 meV at 7 K at 2% doping. For the present discussion, the most important effect of substituting Nb is doping electrons, which yields a clearly distinguishable Drude peak that is broad at 300 K but gets extremely narrow at low temperatures. For the lowest dopings, this can be directly seen from the upturn of  $\epsilon_2(\omega)$  for  $\hbar\omega < 2$  meV (Fig. 1a). For the 0.9% and 2% doped samples, the metallic conductivity is directly visible from the increase of the reflectivity below the soft optical phonon (Fig. 1b). The third effect of doping is the occurrence of a broad asymmetric mid-infrared absorption that increases with doping. At 7 K, a sharper structure shows up on the low-energy side of this band (Fig. 2c-d). Using first principles LDA calculations [16] we have verified that interband transitions within the  $t_{2g}$  manifold are orders of magnitude too weak to account for the observed intensity. We show below that the observed lineshape can be understood as a multiphonon sideband of the free carrier (Drude) response.

As mentioned before, the effective mass of the charge carriers  $m^*$  can be obtained by analyzing the Drude spectral weight. In Fig. 3 we show the spectral weight  $W(\omega)$ , defined as

$$W(\omega_c) \equiv \int_0^{\omega_c} \sigma_1(\omega) d\omega. \quad (1)$$

Neglecting the optical transitions from the core, the electronic contribution  $8W(\infty) = \omega_p^2 = 4\pi ne^2/m$ , where  $e$  and  $m$  are the free electron charge and mass, and  $n$  is the valence electron density. The contribution of the infrared phonons manifests itself in  $W(\omega)$  as steps, *e.g.* at 8.5 meV in the 2% doped sample (Fig. 3). Such a strong phonon close to the Drude peak makes a decomposition of their respective spectral weights challenging, and requires

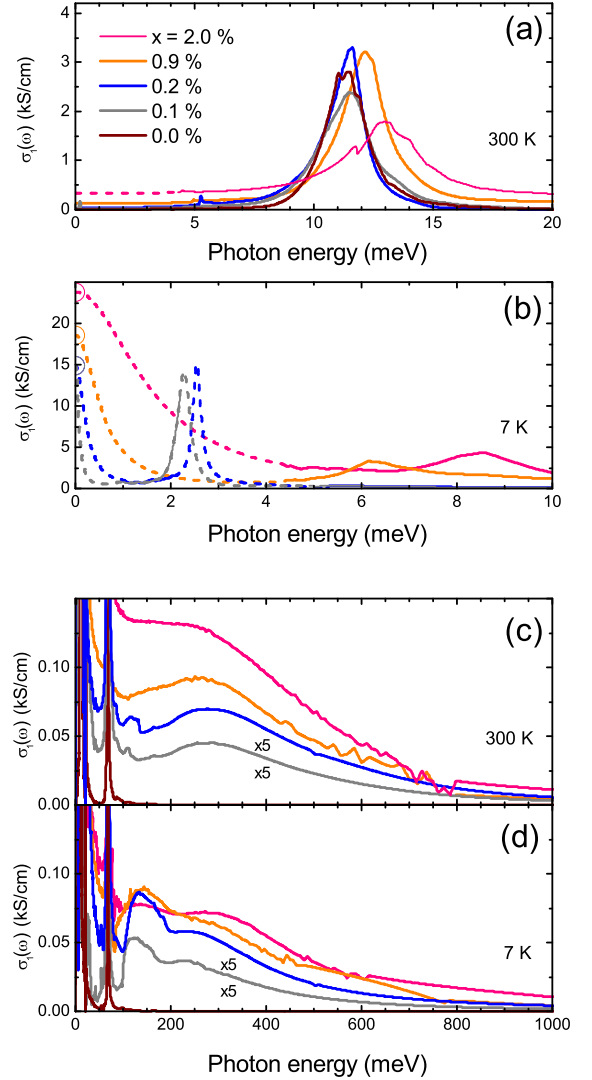


FIG. 2: The optical conductivity of  $\text{SrTi}_{1-x}\text{Nb}_x\text{O}_3$  for  $x = 0, 0.1\%, 0.2\%, 1\%$  and  $2\%$  at 300 and 7 K. The dashed parts of the curves in (a-b) are interpolations fitted to the DC resistivity, reflectivity, transmission and  $\epsilon_1(\omega) + i\epsilon_2(\omega)$  obtained from the THz transmission amplitude and phase. Open symbols are the experimental DC conductivities. (c-d). For clarity, the mid-infrared conductivities of  $x = 0.1\%$  and  $0.2\%$  are magnified by a factor 5.

experimental data that extend beyond the soft phonon frequency unlike previous experimental data. Here, (i) direct measurements of  $\epsilon_1(\omega)$  and  $\epsilon_2(\omega)$  below 3 meV by time-domain THz spectroscopy (for the  $x = 0.1\%$  and  $0.2\%$  samples) and (ii) far-infrared reflectivity between 4 and 10 meV (for the  $x = 0.9\%$  and  $2\%$  samples) shown in Fig. 1 allowed us to extract the Drude spectral weight using several methods.

For the two lowest dopings we apply the partial sum rule (Eq.1) with cutoff frequencies  $\hbar\omega_c = 1.5$  meV ( $0.1\%$ ) and  $2.0$  meV ( $0.2\%$ ), which are larger than the Drude relaxation rate but below the soft phonon (see Fig. 2b) [17],

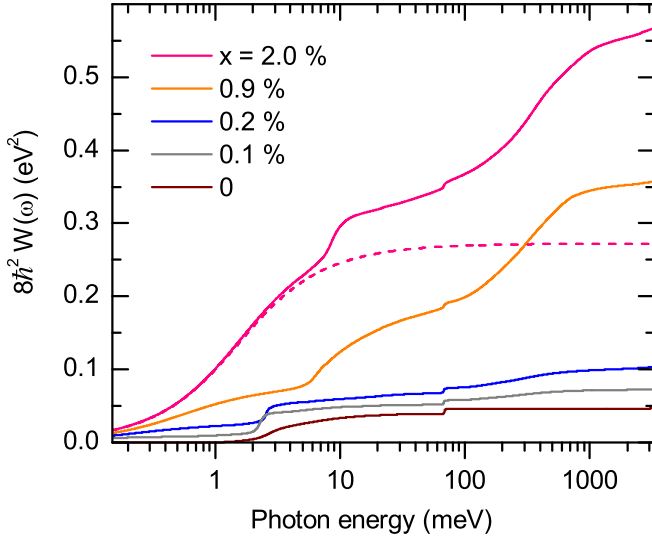


FIG. 3: The integrated optical spectral weight of  $\text{SrTi}_{1-x}\text{Nb}_x\text{O}_3$  as a function of photon energy and relative to the charge carrier concentration, at 7 K. The Drude spectral weight is separately shown for  $x = 2\%$  by the dotted line.

yielding  $\hbar\omega_p = 120 \pm 20$  meV and  $201 \pm 90$  meV, respectively. These values slightly change to  $\hbar\omega_p = 116 \pm 18$  meV and  $159 \pm 23$  meV, respectively, when we carry out a simultaneous Drude-Lorentz fit to these data together with reflectivity and transmission data at higher frequencies and the DC resistivity. For the two higher dopings, no samples transparent in the THz band could be prepared, but the soft-phonon frequency shifts with doping into a range where reliable infrared reflectivity can be obtained, resulting in the dips in reflectivity seen in Fig. 1b. Thus, a standard Kramers-Kronig analysis of the reflectivity can be used as well as Drude-Lorentz fitting. Both methods give essentially identical values,  $\hbar\omega_p = 327 \pm 67$  meV and  $527 \pm 61$  meV for 0.9% and 2% doping, respectively, shown by the red squares in Fig. 4. Defining the mass renormalization of the charge carriers as the ratio of the LDA and the experimental values of the squared plasma-frequency,  $m^*/m_b \equiv \omega_{p,\text{LDA}}^2/\omega_{p,\text{exp}}^2$ , we observe a threefold mass enhancement, *i.e.*,  $m^*/m_b = 2.9 \pm 0.3$  for the low charge carrier densities considered in the present study (Fig. 4, inset).

For  $0.001 \leq x \leq 0.02$ , the band-structure value [18] of the Fermi energy,  $E_F$ , ranges from 0.02 to 0.1 eV, relative to the bottom of the lowest  $t_{2g}$  band, which coincides with the energy of the relevant longitudinal optical phonon,  $\hbar\omega_{\text{LO}} = 0.1$  eV [19, 20]. This is a difficult parameter range to describe theoretically where none of the usual approximations, *i.e.*,  $\hbar\omega_{\text{LO}}/E_F \ll 1$  nor  $\hbar\omega_{\text{LO}}/E_F \gg 1$  are applicable. For the present discussion we consider the latter limit, appropriate for the lower doped samples. It takes as a starting point the model of a single polaron [21, 22], characterized by the

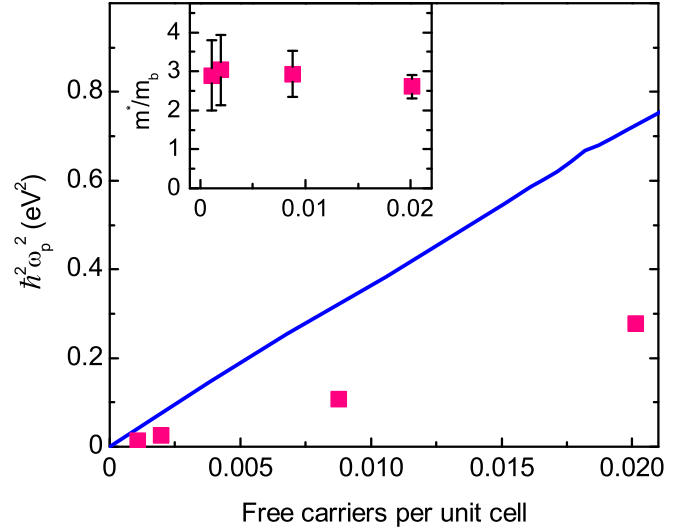


FIG. 4: Experimental plasma frequency at 7 K derived from the spectral weight  $W(\omega)$  of the Drude peak (squares) as a function of the free carrier concentration (from Hall effect) together with that from the band structure calculations [16] (solid line). The inset shows the corresponding effective carrier mass  $m^*/m_b$ .

coupling constant  $\alpha$ . Within a variational approximation, Feynman [21] deduced the relation  $m^*(\alpha)$  valid in the range  $0 < \alpha < 12$ . Applying Feynman's relation to the experimental  $m^*$  values, we obtain a doping independent value of  $\alpha \approx 4$ . This is considerably larger than the value expected for a purely Fröhlich-type interaction, for which (using experimental optical parameters of  $\text{SrTiO}_3$ )  $\alpha = \sqrt{m_b/m_e} \sqrt{Ry/\omega_{\text{LO}}} (\epsilon_\infty^{-1} - \epsilon_s^{-1}) = 2.1$ .

The optical conductivity shows a broad absorption band between 0.1 and 1 eV (Fig. 2c and 2d). The intensity in this mid-infrared band compensates the deficit of Drude spectral weight and the f-sum rule,  $8W(\infty) = \omega_p^2$ , is almost satisfied at 3 eV, as can be seen from Fig. 3 [23]. Such a spectral weight redistribution between the 'coherent' (Drude) and the 'incoherent' (mid-infrared) contributions of the optical conductivity suggests that the mass enhancement reflects coupling of electrons to bosonic degrees of freedom, most probably phonons. A spectral shape similar to the observed mid-infrared band at 300 K (Fig. 2c) was calculated by Emin [24], who considered the photo-ionization spectrum out of the potential well formed by the lattice deformation of the polaron. Upon cooling, the maximum of this band remains between 200 and 350 meV, and at 7K an additional peak emerges on the low-energy side with a maximum varying from 120 (0.1%) to 140 meV (2%). Devreese *et al.* [25, 26, 27] have numerically found a broad mid-infrared band with (for intermediate couplings) a peak at lower energies. They explain it as a multiphonon band and the peak as a relaxed state of an electron optically excited within the polaronic potential well. The model predicts the maxima

of the two bands to be at  $0.065\alpha^2\hbar\omega_{\text{LO}}$  and  $0.14\alpha^2\hbar\omega_{\text{LO}}$ . With the value  $\alpha \approx 4$  that we deduced above this corresponds to 110 meV and 230 meV, consistent with the experimentally observed positions (Fig. 2d).

We conclude that the electron-phonon coupling leads to a threefold mass enhancement in electron doped  $\text{SrTiO}_3$  for charge carrier concentrations between 0.1% and 2% per unit cell. The ‘missing’ Drude spectral weight, as measured directly by THz time-domain transmission spectroscopy, is recovered in the mid-infrared side-bands resulting from the electron-phonon coupling interaction. Analysis of the spectral weight transfer yields a polaronic electron-phonon coupling parameter of intermediate strength,  $\alpha \approx 4$ . This suggests that the charge transport in electron doped  $\text{SrTiO}_3$  could be carried by large polarons. We find no evidence for an extremely strong electron-phonon coupling or small polarons in the considered doping range. Our observations may have important implications for the electron-phonon coupling in perovskites in general, including ferroelectrics, multiferroics, colossal magnetoresistance materials and high- $T_c$  cuprates.

This work was supported by the Swiss National Science Foundation through the NCCR ‘Materials with Novel Electronic Properties’ (MaNEP). NPA has been supported via the NSF’s International Research Fellows program. We gratefully acknowledge stimulating discussions with J.-M. Triscone, K.S. Takahashi, T. Giamarchi, J.T. Devreese, J. Lorenzana and Ø. Fischer.

- 
- [1] A. Lanzara *et al.*, Nature **412**, 510 (2001).
  - [2] A.S. Alexandrov, J. Phys.: Condens. Matter **19**, 125216 (2007).
  - [3] H.Y. Hwang, S.-W. Cheong, P.G. Radaelli, M. Marezio and B. Batlogg, Phys. Rev. Lett. **75**, 914 (1995).
  - [4] N. Mannella *et al.*, Nature **438**, 474 (2005).
  - [5] J.G. Bednorz and K.A. Müller, Rev. Mod. Phys. **60**, 585 (1988).
  - [6] C.S. Koonce, M.L. Cohen, J.F. Schooley, W.R. Hosler and E.R. Pfeiffer, Phys. Rev. **163**, 380 (1967).
  - [7] The low value of  $T_c$  in  $\text{Sr}(\text{Ti},\text{Nb})\text{O}_3$  by no means makes it uninteresting for superconductivity; electron-phonon superconductors with very small carrier density but moderate  $T_c$  may demonstrate an important paradigm of electron-phonon coupling that in a material with more carriers leads to a drastically larger  $T_c$ . Besides the ‘Sleight oxide’ (A.W. Sleight, J.L. Gillson and P.E. Bierstedt, Sol. State Comm. **17**, 27, 1975) one can recall the B-doped diamond (low- $T_c$ ) *vs.*  $\text{MgB}_2$  (same paradigm, larger carrier density, high  $T_c$ ).
  - [8] P. Calvani, Riv. Nuovo Cimento **24**, (2001).
  - [9] D.M. Eagles, M. Georgiev and P.C. Petrova, Phys. Rev. B **54**, 22 (1996).
  - [10] P. Calvani, Phys. Rev. B **47**, 8917 (1993).
  - [11] D.A. Crandles, Phys. Rev. B **59**, 12842 (1999).
  - [12] F. Gervais, J.-L. Servoin, A. Baratoff, J.G. Bednorz and G. Binnig, Phys. Rev. B **47**, 8187 (1993).
  - [13] A.S. Barker Jr., *Optical Properties and Electronic Structure of Metals and Alloys*, 452-468 (ed. F. Abelès, North-Holland, Amsterdam, 1965).
  - [14] C.Z. Bi *et al.*, J. Phys.: Condens. Matter **18**, 2553 (2006).
  - [15] A.B. Kuzmenko, Rev. Sci. Instrum. **76**, 083108 (2005).
  - [16] We employed the Linear Augmented Plane Wave method as implemented in the WIEN2k code (WIEN2k, An Augmented Plane Wave +Local Orbitals Program for Calculating Crystal Properties, Karlheinz Schwarz, Techn. Universität Wien, Austria, 2001) and the generalized gradient approximation for the exchange-correlation potential in the form proposed by J.P. Perdew, K. Burke, and M. Ernzerhof (Phys. Rev. Lett. **77**, 3865, 1996). Calculations have been performed in the high-temperature perovskite structure ( $a = 3.905 \text{ \AA}$ ) as well as in the low-temperature tetragonal structure (group #140, 14/mcm,  $a = 5.529 \text{ \AA}$ ,  $c = 7.824 \text{ \AA}$ ,  $O_x = 0.244$ ); optimizing the O position in the calculations yields  $O_x = 0.223$ , indicating, not surprisingly, that even zero-point fluctuations substantially reduce the average distortion. Nb doping was simulated by changing the nuclear charge of Ti from 22 to  $22 + x$ , or that of Sr from 38 to  $38 + x$  (the results did not change, proving that this is a good approximation in the considered range of dopings). Fermi-surface integrals were evaluated using the k-point meshes up to  $28 \times 28 \times 28$ . The Fermi velocities (for the  $\omega_p$  calculations) and optical matrix elements were calculated using the WIEN2k optics package.
  - [17] We used a novel algorithm (A.B. Kuzmenko, D. van der Marel, F. Carbone and F. Marsiglio, cond-mat/0701593) that allows a direct, model-independent, extraction of  $W(\omega_c)$  from  $\epsilon_1(\omega)$  and  $\epsilon_2(\omega)$  measured in a limited range.
  - [18] Note that our first principles results show a substantially weaker effect of the tetragonality compared to the generally used semi-empirical calculations of Mattheiss [28] (less than 4 meV splitting of the otherwise degenerate states at  $\Gamma$ , compared to  $\sim 20$  meV). This in fact resolves a long-standing controversy between the accepted band structure of Ref. [28] and the de Haas-van Alphen measurements of Gregory *et al.* [29].
  - [19] J.-L. Servoin, Y. Luspain and F. Gervais, Phys. Rev. B **22**, 5501 (1980).
  - [20] G. Verbist, F.M. Peeters and J.T. Devreese, Ferroelectrics **130**, 27 (1992).
  - [21] R.P. Feynman, Phys. Rev. **97**, 660 (1955).
  - [22] G.D. Mahan, *Many-particle physics*, Plenum, New York, (1990).
  - [23] In order to account for the lattice vibrational contributions (assumed to be doping independent) to the sum rule at  $\omega_c = 3 \text{ eV}$  we subtracted, for all dopings, the corresponding value of undoped  $\text{SrTiO}_3$ .
  - [24] D. Emin, Phys. Rev. B **48**, 13691 (1993).
  - [25] E. Kartheuser, R. Evrard and J. Devreese, Phys. Rev. Lett. **22**, 94 (1969).
  - [26] J. Devreese, J. de Sitter and M. Goovaerts, Phys. Rev. B **5** 2367 (1972).
  - [27] G. Iadonisi, Riv. Nuovo Cimento **7**, 1 (1984).
  - [28] L.F. Mattheiss, Phys. Rev. B **6**, 4740 (1972).
  - [29] B. Gregory, J. Arthur, and G. Seidel, Phys. Rev. B **19**, 1039 (1979).